

Numerical solution of the Boltzmann equation for the collective modes of trapped Fermi gases.

Thomas Lepers* and Dany Davesne

Université de Lyon, F-69622 Lyon, France; Univ. Lyon 1, Villeurbanne; CNRS/IN2P3, UMR5822, IPNL

Silvia Chiacchiera

*Centro de Física Computacional, Department of Physics,
University of Coimbra, P-3004-516 Coimbra, Portugal*

Michael Urban

Institut de Physique Nucléaire, CNRS/IN2P3 and Université Paris-Sud 11, 91406 Orsay Cedex, France

(Dated: April 29, 2010)

We numerically solve the Boltzmann equation for trapped fermions in the normal phase using the test-particle method. After discussing a couple of tests in order to estimate the reliability of the method, we apply it to the description of collective modes in a spherical harmonic trap. The numerical results are compared with those obtained previously by taking moments of the Boltzmann equation. We find that the general shape of the response function is very similar in both methods, but the relaxation time obtained from the simulation is significantly longer than that predicted by the method of moments. It is shown that the result of the method of moments can be corrected by including fourth-order moments in addition to the usual second-order ones and that this method agrees very well with our numerical simulations.

PACS numbers: 67.85.Lm,02.70.Ns

I. INTRODUCTION

In experiments on ultracold trapped Fermi gases, there are many situations where the system is out of thermal equilibrium. The first one is of course the trapping and cooling stage, i.e., before the system has reached its equilibrium state which is usually the starting point for the actual experiment. Then, in some experiments the system is excited in order to observe its dynamical behavior. For instance, many experiments studied collective oscillations of the system [1–7], another example being a recent experiment at MIT where the collision of two atom clouds (both in equilibrium) was studied [8]. Finally, often the system is not imaged directly during the experiment, but only after the trap was switched off and the system has expanded for a certain time, in order to increase its size.

The modeling of such time-dependent processes from the theoretical point of view can be quite complicated. For practical reasons, only semiclassical approaches are suitable for the description of time-dependent phenomena involving typically several 10^5 atoms in a three-dimensional, non-uniform geometry. In some cases, it is possible to use hydrodynamic approaches: Superfluid hydrodynamics describes the expansion [9] and the collective modes [10] of superfluid systems at zero temperature. Hydrodynamics is also applicable in the normal-fluid phase if the mean time between collisions is much shorter than all other time scales of the process under consideration, so that the system can always be consid-

ered to be in a local equilibrium [10, 11]. Superfluid and normal hydrodynamics can be combined to two-fluid hydrodynamics in order to describe superfluid systems at finite temperature [12]. However, in many cases hydrodynamic approaches are not sufficient. In all cases where it is important that even locally the distribution $f(\mathbf{r}, \mathbf{p}, t)$ of the atoms is not an equilibrium one, the Boltzmann equation allows a very general description, provided the system is in the normal phase. If the system is superfluid, a more elaborate theory is necessary which couples the dynamics of the quasiparticle distribution function to the dynamics of the superfluid order parameter [13, 14].

In the past, several authors used the Boltzmann equation for the investigation of collective oscillations in normal-fluid trapped Fermi gases [6, 11, 15–19]. In most cases, the Boltzmann equation was not solved directly in order to find the distribution function f , but semi-analytical approximate solutions were found by using the scaling ansatz [11] or the method of moments [6, 17–19]. These methods rely explicitly or implicitly on the assumption that the collision term can be treated in the relaxation-time approximation, with a single relaxation time τ which is independent of the position in the trap. An exception is the work by Toschi et al. [15, 16], where the Boltzmann equation was solved numerically, using a test-particle method very similar to the one we are using here. The test-particle method for the solution of the Boltzmann equation has been used for many years in nuclear physics for the simulation of heavy-ion collisions [20]. In the context of trapped atoms, it was also used for the simulation of the dynamics of the thermal cloud in a Bose-Einstein condensate [21] and (without collision term) of the normal-fluid component in a superfluid

*Electronic address: t.lepers@ipnl.in2p3.fr

Fermi gas [14].

For the collision term of the Boltzmann equation, it is important to know the cross section which in principle can be modified by in-medium effects. In the work by Riedl et al. [6], it was shown that by using in the Boltzmann equation instead of the free cross-section the in-medium one, the agreement between theoretical and experimental frequencies and damping rates of different collective modes is deteriorated. The reason is that the in-medium cross section is larger than the free one, so that the relaxation time is dramatically reduced. In our previous work [19], our aim was to include in addition to the in-medium cross section medium effects into the mean-field potential. This mean field resulted in better density profiles and allowed us to understand the shift of the quadrupole frequency in the collisionless regime at very low temperature observed in [4]. However, it did not help to improve the agreement between theory and experiment in the region of higher temperatures, where the properties of the collective modes are completely dominated by collisions.

Hence, one of our motivations for the present work was to check the validity of the relaxation-time approximation which is implicitly made in the method of moments. Here we will restrict ourselves to the case without mean field and with the free cross section. As we will show in Sec. III, the numerical solution of the Boltzmann equation gives indeed a significantly longer relaxation time than the method of moments. As we will show, this discrepancy is due to the restriction of the method of moments to second-order moments in the existing literature [6, 17–19]. Once fourth-order moments are included, the results of the method of moments and of the numerical solution are in good agreement. However, already in the simplest case of a spherical harmonic trap without mean field, the inclusion of fourth-order moments is a very tedious task, while the numerical method can be generalized to more realistic cases.

In addition, there are some other reasons why we felt the necessity for a numerical method. For example, there are damping effects due to the anharmonicity of the trap potential which cannot be described by the method of moments. Another advantage of the numerical method is that it offers the possibility to simulate not only the oscillation of the cloud, but also the subsequent expansion after the trap has been switched off.

In Sec. II of the present paper, we give a detailed description of the method. In particular, we explain in detail how the collisions are simulated, since our method is somewhat different from that of Ref. [15]. Moreover we discuss some tests we made in order to estimate up to which precision we can trust our simulation. Then, in Sec. III, we come to the main point of our article and calculate the properties of some collective modes for a system in a spherical harmonic trap. While the sloshing and breathing modes are rather trivial, the frequency and damping rate of the quadrupole mode are very sensitive to the collisions. We compare the numerical results with

those of the method of moments. Finally, in Sec. IV we summarize and give an outlook to future studies.

Throughout the paper, we will use units with $\hbar = k_B = 1$ ($\hbar =$ reduced Planck constant, $k_B =$ Boltzmann constant). The strength of the interaction is characterized by the dimensionless quantity $k_F a$, where a is the scattering length. Concerning the Fermi momentum k_F and the Fermi energy E_F we follow the usual convention that these quantities are defined by the corresponding ones of an ideal Fermi gas at zero temperature, i.e., $k_F = \sqrt{2mE_F}$, m being the atomic mass, and $E_F = (3N)^{1/3}\omega_0$, where N is the number of atoms and ω_0 the trap frequency. Temperatures will be measured in units of the Fermi temperature $T_F = E_F$ (since $k_B = 1$).

II. DESCRIPTION OF THE NUMERICAL METHOD

A. Test-particle method

We study a two-component ($\sigma = \uparrow, \downarrow$) gas of fermionic atoms of mass m in a potential $V(\mathbf{r}, t)$ with attractive interaction $a < 0$. We assume that the system is in the normal phase and that it can be described semiclassically by phase-space distribution functions $f_\sigma(\mathbf{r}, \mathbf{p}, t)$. In this paper, we will restrict ourselves to the case that the distribution functions of both spin states are equal ($f_\uparrow = f_\downarrow = f$), but the generalization of the method to the cases of different distribution functions, more than two components, or components with different masses is straight-forward.

The time evolution of the distribution function f is governed by the Boltzmann equation [22]

$$\dot{f} + \dot{\mathbf{r}} \cdot \nabla_{\mathbf{r}} f + \dot{\mathbf{p}} \cdot \nabla_{\mathbf{p}} f = -I[f], \quad (1)$$

where the left-hand side (lhs) describes the particle propagation, with

$$\dot{\mathbf{r}} = \frac{\mathbf{p}}{m} \quad \text{and} \quad \dot{\mathbf{p}} = -\nabla V, \quad (2)$$

and $I[f]$ on the right-hand side (rhs) denotes the collision term which will be discussed later. The potential felt by the particles is the trap potential that contains a static part and a time dependent one (which will be used to simulate the excitation of the collective modes) $V(\mathbf{r}, t) = V_T(\mathbf{r}) + V_1(\mathbf{r}, t)$.

The density per spin state is related to the distribution function by

$$\rho(\mathbf{r}, t) = \int \frac{d^3 p}{(2\pi)^3} f(\mathbf{r}, \mathbf{p}, t), \quad (3)$$

and the number of atoms is given by

$$N = N_\uparrow + N_\downarrow = 2 \int d^3 r \rho(\mathbf{r}, t). \quad (4)$$

The basic idea of the test-particle method (also called pseudoparticle method) for solving the Boltzmann equation consists in replacing the continuous distribution function by a sum of delta functions,

$$f(\mathbf{r}, \mathbf{p}, t) = \frac{N}{2\tilde{N}} \sum_{i=1}^{\tilde{N}} (2\pi)^3 \delta(\mathbf{p} - \mathbf{p}_i(t)) \delta(\mathbf{r} - \mathbf{r}_i(t)), \quad (5)$$

where \tilde{N} is the number of “test particles”. This allows one to express the average of an arbitrary single-particle observable $F(\mathbf{r}, \mathbf{p})$ in the simple form

$$\langle F \rangle = \frac{2}{N} \int \frac{d^3r d^3p}{(2\pi)^3} f(\mathbf{r}, \mathbf{p}, t) F(\mathbf{r}, \mathbf{p}) = \frac{1}{\tilde{N}} \sum_{i=1}^{\tilde{N}} F(\mathbf{r}_i, \mathbf{p}_i). \quad (6)$$

In order to sample the six-dimensional phase space, it is necessary to choose a sufficiently large number of test particles \tilde{N} (usually $\tilde{N} > N$). Neglecting the collision term $I[f]$ for the moment, it is easy to see that Eq. (5) satisfies the Boltzmann equation (Eq. (1)) if the positions \mathbf{r}_i and momenta \mathbf{p}_i of each test particle i follow the classical equations of motion, Eq. (2).

In practice, the delta functions in Eq. (5) can pose some problems. For instance, they do not result in a continuous density $\rho(\mathbf{r})$. Therefore it is often useful to replace them by Gaussians of width w_r and w_p in position and momentum space, respectively:

$$\delta(\mathbf{p} - \mathbf{p}_i) \delta(\mathbf{r} - \mathbf{r}_i) \rightarrow g_{w_p}(\mathbf{p} - \mathbf{p}_i) g_{w_r}(\mathbf{r} - \mathbf{r}_i), \quad (7)$$

with

$$g_{w_p}(\mathbf{p}) = \frac{e^{-p^2/w_p^2}}{(\sqrt{\pi}w_p)^3} \quad \text{and} \quad g_{w_r}(\mathbf{r}) = \frac{e^{-r^2/w_r^2}}{(\sqrt{\pi}w_r)^3}. \quad (8)$$

The widths w_r and w_p must be adapted such that they smooth out the fluctuations due to the finite number of test particles, but not the structure of the distribution function f . The statistical fluctuations are of the order of $(2\tilde{N}w_r^3w_p^3/N)^{-1/2}$, i.e., the first condition is equivalent to

$$w_r w_p \gg \left(\frac{N}{2\tilde{N}} \right)^{1/3}. \quad (9)$$

The second condition implies of course that $w_r \ll R_{TF}$ and $w_p \ll p_F$, where R_{TF} and p_F are the Thomas-Fermi radius and the Fermi momentum, respectively, but this is not always sufficient. At low-temperature, it is crucial to resolve the rapid change of the distribution function around the Fermi surface, i.e.,

$$w_p \ll p_F \frac{T}{T_F} \quad \text{and} \quad w_r \ll R_{TF} \frac{T}{T_F}. \quad (10)$$

In practice, as the computation time increases as \tilde{N}^2 , it turns out that the conditions (9) and (10) cannot simultaneously be satisfied at too low temperatures.

B. Particle propagation

In the absence of collisions, the numerical task consists only in solving simultaneously the classical equations of motion (2) for the \tilde{N} test particles. We do this by using the velocity Verlet algorithm [24], which contrary to the original Verlet algorithm [25] uses the positions $\mathbf{r}_i(t_n)$ and velocities $\mathbf{v}_i(t_n) = \dot{\mathbf{p}}_i(t_n)/m$ as starting point for the time step from t_n to $t_{n+1} = t_n + \Delta t$. The propagation from t_n to t_{n+1} is done according to

$$\mathbf{v}_i(t_{n+1/2}) = \mathbf{v}_i(t_n) + \mathbf{a}_i(t_n) \Delta t / 2 \quad (11)$$

$$\mathbf{r}_i(t_{n+1}) = \mathbf{r}_i(t_n) + \mathbf{v}_i(t_{n+1/2}) \Delta t \quad (12)$$

$$\mathbf{v}_i(t_{n+1}) = \mathbf{v}_i(t_{n+1/2}) + \mathbf{a}_i(t_{n+1}) \Delta t / 2, \quad (13)$$

where $\mathbf{a}_i(t) = -\nabla V(\mathbf{r}_i(t), t)/m$ is the acceleration of the i -th test particle. If it is written in this way, it is obvious that the velocity Verlet algorithm is identical to the leap-frog algorithm [26]. Note that the accelerations $\mathbf{a}_i(t_{n+1})$ can be reused in the next time step, so that the algorithm needs only one evaluation of the acceleration per time step, but nevertheless its global error is of the order $\mathcal{O}(\Delta t)^2$. This allows us to obtain a good accuracy for reasonable time steps Δt . A good test of the particle propagation is to check the energy conservation: typically we find $|E_i(t) - E_i(0)|/E_i(0) \simeq 10^{-6}$ for each test particle and for all times considered.

C. Collision term

The rhs of the Boltzmann equation (1) describes the collisions between particles of opposite spin. It thus depends on the scattering cross section $d\sigma/d\Omega$ and reads [22]

$$I[f] = \int \frac{d^3p_1}{(2\pi)^3} \int d\Omega \frac{d\sigma}{d\Omega} |\mathbf{v} - \mathbf{v}_1| [f f_1 (1 - f')(1 - f'_1) - f' f'_1 (1 - f)(1 - f_1)]. \quad (14)$$

In the first term, \mathbf{p} and \mathbf{p}_1 are the incoming momenta, \mathbf{p}' and \mathbf{p}'_1 are the outgoing ones, Ω is the solid angle formed by the incoming relative momentum $\mathbf{p} - \mathbf{p}_1$ and the outgoing relative momentum $\mathbf{p}' - \mathbf{p}'_1$, and $f \equiv f(\mathbf{r}, \mathbf{p}, t)$, $f_1 \equiv f(\mathbf{r}, \mathbf{p}_1, t)$, etc. In the second term, the role of incoming and outgoing momenta is exchanged. Momentum and energy conservation implies $\mathbf{p} + \mathbf{p}_1 = \mathbf{p}' + \mathbf{p}'_1$ and $|\mathbf{p} - \mathbf{p}_1| = |\mathbf{p}' - \mathbf{p}'_1|$. Here we consider the case of pure s -wave scattering, in which the cross section is isotropic, i.e., $d\sigma/d\Omega = \sigma/4\pi$. In principle the cross section is modified by medium effects [18, 19], but in the present paper we will only use the free cross-section (i.e., the cross-section for the scattering of two atoms of opposite spin in free space) which is given by [23]

$$\sigma = \frac{4\pi a^2}{1 + (qa)^2}, \quad (15)$$

where $q = |\mathbf{p} - \mathbf{p}_1|/2 = |\mathbf{p}' - \mathbf{p}'_1|/2$.

In our numerical simulation, the collision term is included by allowing the test particles to collide with each other. The cross section of the test particles, $\tilde{\sigma}$, is related to the cross section of the atoms by $\tilde{\sigma} = \sigma N/2\tilde{N}$ (since \tilde{N} test particles represent $N/2$ atoms of a given spin). Whether a pair i, j of test particles collides in a time step t_n or not is determined as follows: First, we determine if the two particles are at their closest approach in the present time step. Explicitly, if we write $\mathbf{r}_{ij} = \mathbf{r}_i - \mathbf{r}_j$ and $\mathbf{v}_{ij} = \mathbf{v}_i - \mathbf{v}_j$, the closest approach is reached at $t_{min} = t_n - \mathbf{r}_{ij} \cdot \mathbf{v}_{ij}/v_{ij}^2$ and we check if $|t_{min} - t_n| < \Delta t/2$. If yes, we calculate the corresponding minimal distance by $d_{min}^2 = r_{ij}^2 - (\mathbf{r}_{ij} \cdot \mathbf{v}_{ij})^2/v_{ij}^2$ and check if $\pi d_{min}^2 < \tilde{\sigma}$. In this case, the collision is classically allowed. We then propagate both test particles to t_{min} , change the direction of their relative velocity \mathbf{v}_{ij} in a random way (thus conserving the total momentum and the total energy), and propagate them back to the original time t_n . Finally, in order to take into account the Pauli-blocking factors in Eq. (14), we calculate the occupation numbers f'_i and f'_j at the new positions and momenta ($f'_i = f(\mathbf{r}'_i, \mathbf{p}'_i)$ etc.) using Eq. (5) with Gaussians instead of delta functions, see Eq. (7). With probability $(1 - f'_i)(1 - f'_j)$ the collision is allowed and we keep the new positions and momenta, otherwise the collision is blocked and we keep the old ones.

We checked that the total energy is still well conserved when collisions are switched on: typically we find better than $|\langle E \rangle(t) - \langle E \rangle(0)|/\langle E \rangle(0) \simeq 10^{-5}$ for all times considered.

D. Initialization

Before the simulation can start, the test-particle positions and momenta have to be initialized. Here we assume that the system is initially in equilibrium.

A suitable equilibrium distribution is given by the distribution function within the Thomas-Fermi or local-density approximation (LDA),

$$f_{eq}(\mathbf{r}, \mathbf{p}) = \frac{1}{e^{\beta(p^2/2m + V_T(\mathbf{r}) - \mu)} + 1}, \quad (16)$$

since it is a stationary solution of the Boltzmann equation [22]. This distribution has two parameters, namely the inverse temperature $\beta = 1/T$ and the chemical potential μ . The temperature T is an input parameter, whereas the chemical potential μ is determined by demanding that the integral of Eq. (16) over \mathbf{r} and \mathbf{p} gives the right number of atoms.

Having determined the chemical potential μ , we randomly generate the test-particle positions and momenta in such a way that the probability to be at position \mathbf{r} and to have momentum \mathbf{p} is proportional to $f_{eq}(\mathbf{r}, \mathbf{p})$. In practice, we do this by first generating the positions according to the density profile obtained from Eq. (3) with

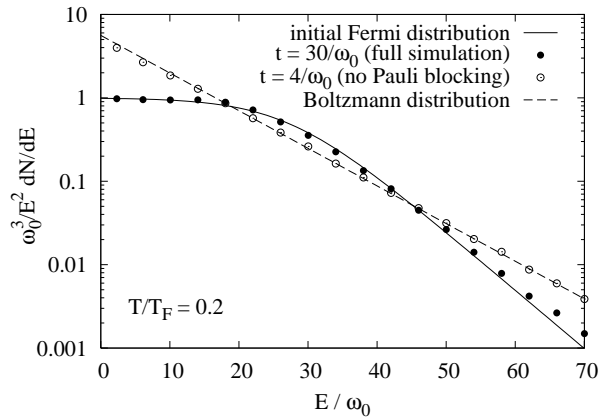


FIG. 1: Energy distribution of the atoms (divided by the density of states) for $T/T_F = 0.2$ (see text for details). The system consists of $N = 10000$ atoms with a scattering length $a = -0.2537l_{ho}$ ($1/(k_F a) = -0.5$). The parameters of the simulation are: $\tilde{N} = 50000$, $w_r = 1.5l_{ho}$, $w_p = 1.5/l_{ho}$, and $\Delta t = 0.02/\omega_0$.

$f = f_{eq}$. Then we generate the momenta according to f_{eq} .

E. Tests of reliability and accuracy

In this subsection we describe two main tests we made to be sure that our code is reliable. Here, we assume the potential to be static and, as in the rest of the paper, we use a spherical harmonic potential

$$V(\mathbf{r}, t) = V_T(\mathbf{r}) = \frac{1}{2}m\omega_0^2 r^2. \quad (17)$$

This potential defines naturally a time scale $1/\omega_0$, a length scale $l_{ho} = 1/\sqrt{m\omega_0}$, an energy scale ω_0 , and so on.

Let us consider the energy distribution of the atoms,

$$\frac{dN}{dE} = 2 \int \frac{d^3r d^3p}{(2\pi)^3} f(\mathbf{r}, \mathbf{p}) \delta\left(\frac{p^2}{2m} + V_T(\mathbf{r}) - E\right). \quad (18)$$

In equilibrium, the distribution should be given by $dN/dE = g(E)/(e^{(E-\mu)/T} + 1)$, where $g(E)$ is the density of states (including the degeneracy factor 2). In the present case of a spherical harmonic oscillator, we have $g(E) = E^2/\omega_0^3$. In the absence of collisions, energy conservation automatically implies that the distribution stays constant, but in the presence of collisions this test is a non-trivial check of the Pauli blocking in the simulation. Within the test particle method, dN/dE is obtained by counting the test particles in energy bins.

In Fig. 1 we show, for $T/T_F = 0.2$, the initial Fermi distribution (solid line) and the stationary distribution obtained in the numerical simulation after $t = 30/\omega_0$ (filled circles). The agreement between the distribution

generated by the simulation and the initial Fermi one is not perfect, but satisfactory. In order to show that this is not a trivial result, let us see what happens if we switch off the Pauli blocking in the simulation of the collision term. In this case, already after a relatively short time $\sim 3/\omega_0$, the distribution in the numerical simulation (empty circles) has converged to a Boltzmann distribution with the same number of atoms and total energy (dashed line). So, the stability of the Fermi distribution in our full simulation shows clearly that Pauli blocking is correctly implemented. The small deviations from the ideal Fermi distribution are a consequence of the fact that with the chosen widths of the Gaussians ($w_r = 1.5l_{ho}$ and $w_p = 1.5/l_{ho}$), the condition (10) is not well satisfied at $T/T_F = 0.2$. When we did the same kind of comparison at higher temperatures, we found that the agreement between the simulation and the Fermi distribution improves: at $T/T_F = 0.4$, it is already perfect.

The test described above is independent of the actual number of collisions. In order to check the latter, let us look at the collision rate

$$\dot{N}_{coll} = \int d^3r \int \frac{d^3p}{(2\pi)^3} \int \frac{d^3p_1}{(2\pi)^3} \int d\Omega \frac{d\sigma}{d\Omega} |\mathbf{v} - \mathbf{v}_1| \times f f_1 (1 - f') (1 - f'_1). \quad (19)$$

In the numerical simulation, this quantity can be obtained as $\dot{N}_{coll} = (N/\tilde{N})\dot{\tilde{N}}_{coll}$, where $\dot{\tilde{N}}_{coll}$ denotes the number of collisions of test particles per unit time.

Although in equilibrium the net effect of collisions is zero, the collision rate in equilibrium is a good test for the simulation because it can be compared with the exact result [Eq. (A1), see Appendix A]. For testing purposes, it is useful to compare also the total rate of allowed and blocked collisions with the exact result [Eq. (A2)].

In Fig. 2, the collision rates (with and without blocking) of the simulation are shown together with the exact results as functions of the temperature for two different values of the scattering length. In the case of relatively weak interaction, $1/k_F a = -1$ (upper panel), we see that the agreement between the simulation and the exact result is excellent for temperatures above $\sim 0.35 T_F$. Below that temperature, the collision rate in the simulation with Pauli blocking gradually becomes too high since the finite widths of the Gaussians ($w_r = 1.5l_{ho}$, $w_p = 1.5/l_{ho}$) do not satisfy any more the condition (10) and act in the Pauli-blocking factors like an enhanced temperature. In the rest of this paper, we will therefore restrict ourselves to temperatures above $0.2 T_F$. Near unitarity ($1/k_F a = -0.1$), we consider only temperatures above $0.3 T_F$ because this is close to the superfluid transition temperature at unitarity [19]. As it can be seen in the lower panel of Fig. 2, the agreement between the collision rate obtained in the simulation and the exact one is satisfactory in the temperature range considered. The agreement is not as good as for $1/k_F a = -1$ at high temperature because of the larger cross section which leads to collisions between test particles which are further apart.

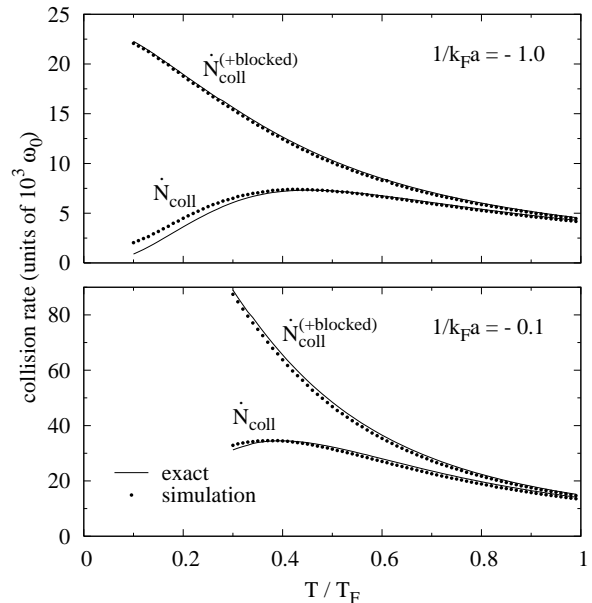


FIG. 2: Simulated collision rates (filled circles) with and without blocking compared with the corresponding exact results, Eqs. (A1) and Eq. (A2) (solid lines), for a gas of 10000 atoms with interaction strength $1/k_F a = -1.0$ (top) and -0.1 (bottom).

III. SIMULATION OF COLLECTIVE MODES

A. Sloshing mode

The sloshing mode is an oscillation of the center of mass of the system. It plays a special role because in a harmonic trap it is undamped and its frequency is equal to that of the trap, independently of the number of atoms, of the temperature, and of the interaction between the atoms (Kohn mode [27, 28]). This is why it is often used for the experimental determination of the trap frequency [5]. Within the test-particle method, this general theorem is satisfied and it is easy to see why:

Let us first neglect collisions. From the equations of motion of the individual test particles in the harmonic potential (17),

$$\dot{\mathbf{r}}_i = \mathbf{p}_i/m \quad \text{and} \quad \dot{\mathbf{p}}_i = -m\omega_0^2 \mathbf{r}_i \quad (20)$$

it is evident that the averages $\langle \mathbf{r} \rangle$ and $\langle \mathbf{p} \rangle$ obey analogous equations of motion,

$$\frac{d}{dt} \langle \mathbf{r} \rangle = \frac{\langle \mathbf{p} \rangle}{m} \quad \text{and} \quad \frac{d}{dt} \langle \mathbf{p} \rangle = -m\omega_0^2 \langle \mathbf{r} \rangle. \quad (21)$$

Let us now consider the effect of a collision of two test particles. Of course, the trajectories of the colliding test particles will not obey any more the original equations of motion (20), but the collision has absolutely no effect on the averages: Since the positions do not change during the collision, $\langle \mathbf{r} \rangle$ remains unchanged, and since the total momentum of the two colliding test particles is conserved,

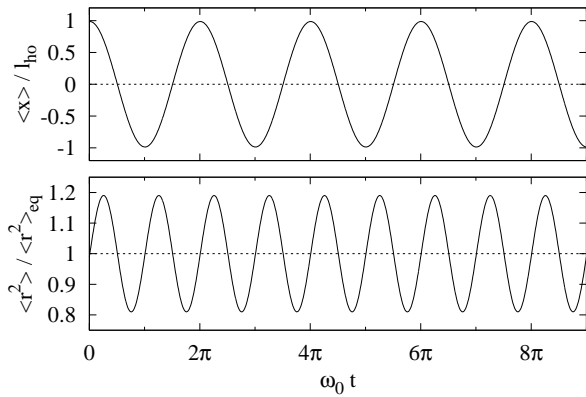


FIG. 3: Top: simulation of the sloshing mode. The mode was excited at $t = 0$ by displacing all test particles by l_{ho} in the x direction. Bottom: simulation of the breathing mode. The mode was excited by changing at $t = 0$ all test-particle momenta according to $\mathbf{p}_i \rightarrow \mathbf{p}_i + c\mathbf{r}_i$ ($c = 0.2m\omega_0$). Both simulations were done for a system of $N = 5000$ particles at $T = 0.4T_F$ and $1/k_F a = -0.3$.

the average $\langle \mathbf{p} \rangle$ is not changed either. So, the equations of motion (21) for the averages $\langle \mathbf{r} \rangle$ and $\langle \mathbf{p} \rangle$ remain valid in the presence of collisions. Their solution is of course an undamped oscillation of the center of mass $\langle \mathbf{r} \rangle$ with frequency ω_0 . This is confirmed by the numerical result shown in the upper panel of Fig. 3.

B. Breathing mode

A couple of experiments studied the damping of the longitudinal and radial breathing modes [1–3, 5, 6] in elongated traps. In a spherical trap, there is only one breathing mode (monopole mode), corresponding to an oscillation of the mean-square radius $\langle r^2 \rangle$ around its equilibrium value $\langle r^2 \rangle_{eq}$. In a spherical harmonic trap, this mode is undamped and its frequency $2\omega_0$ is independent of the number of collisions, like in the case of the sloshing mode.

Again, this is easy to see. Consider the average kinetic and potential energies, $\langle E_{kin} \rangle = \langle p^2 \rangle / 2m$ and $\langle E_{pot} \rangle = m\omega_0^2 \langle r^2 \rangle / 2$. In equilibrium, both are equal (virial theorem). Now let us assume that the system is compressed or expanded, such that $\langle E_{kin} \rangle \neq \langle E_{pot} \rangle$. Using again the equations of motion (20), one obtains

$$\frac{d}{dt}(\langle E_{kin} \rangle - \langle E_{pot} \rangle) = -2\omega_0^2 \langle \mathbf{r} \cdot \mathbf{p} \rangle, \quad (22)$$

$$\frac{d}{dt} \langle \mathbf{r} \cdot \mathbf{p} \rangle = 2(\langle E_{kin} \rangle - \langle E_{pot} \rangle). \quad (23)$$

Obviously, these two equations describe an undamped oscillation with frequency $2\omega_0$. Let us now look if they stay valid in the presence of collisions. Since the collisions do not change the positions of the particles and conserve the total kinetic energy, it is clear that $\langle E_{kin} \rangle$ and $\langle E_{pot} \rangle$

are not affected. Now let us write the difference of $\langle \mathbf{r} \cdot \mathbf{p} \rangle$ before and after a collision of two test particles i and j :

$$\langle \mathbf{r} \cdot \mathbf{p} \rangle' - \langle \mathbf{r} \cdot \mathbf{p} \rangle = \frac{1}{N} \mathbf{r}_{ij} \cdot (\mathbf{q}'_{ij} - \mathbf{q}_{ij}), \quad (24)$$

where \mathbf{q}_{ij} and \mathbf{q}'_{ij} are the relative momenta (e.g., $\mathbf{q}_{ij} = (\mathbf{p}_i - \mathbf{p}_j)/2$) before and after the collision. In the original collision term as written in Eq. (14), particles have to be at the same position to collide, i.e., $\mathbf{r}_{ij} = 0$, such that $\langle \mathbf{r} \cdot \mathbf{p} \rangle$ is not changed. In our simulation this is somewhat different, since the test particles can collide at a distance of up to $\sqrt{\sigma}/\pi$. This adds a small noise to $\langle \mathbf{r} \cdot \mathbf{p} \rangle$. In all practical cases, however, this noise is completely negligible. As an example we show in the lower panel of Fig. 3 the oscillation of the mean-square radius of the cloud as a function of time. As one can see, it is a perfectly undamped harmonic oscillation with frequency $2\omega_0$.

C. Excitation of an arbitrary mode

For the theoretical investigation of collective modes, it is convenient to consider a system which is in equilibrium until it is excited by a short pulse at $t = 0$. Formally, this is achieved by adding to the time-independent trap potential a perturbation term of the form

$$V_1(\mathbf{r}, t) = \hat{V}_1(\mathbf{r})\delta(t). \quad (25)$$

The reason for this choice, which is of course different from the experimental way of exciting a collective mode, is the following: Provided the perturbation \hat{V}_1 is small enough (such that the system reacts linearly to it), the response to a perturbation with arbitrary time dependence, $V_1(\mathbf{r}, t) = \hat{V}_1(\mathbf{r})F(t)$, can easily be obtained by folding the result for the perturbation (25) with the function $F(t)$.

By integrating the Boltzmann equation over the (infinitesimal) duration of the pulse, one can show that the effect of the perturbation (25) is to change the distribution function as

$$f(\mathbf{r}, \mathbf{p}, 0^+) = f(\mathbf{r}, \mathbf{p} + \nabla \hat{V}_1(\mathbf{r}), 0^-), \quad (26)$$

where 0^+ and 0^- denote the limits $t \rightarrow 0$ from above and below, respectively. In the numerical simulation, this means that all test particles get a kick at $t = 0$,

$$\mathbf{p}_i(0^+) = \mathbf{p}_i(0^-) - \nabla \hat{V}_1(\mathbf{r}_i(0)) \quad (27)$$

whereas their positions are not changed by the perturbation.

D. Quadrupole mode

From now on we will study the quadrupole mode as an example for a collective mode with non-trivial properties.

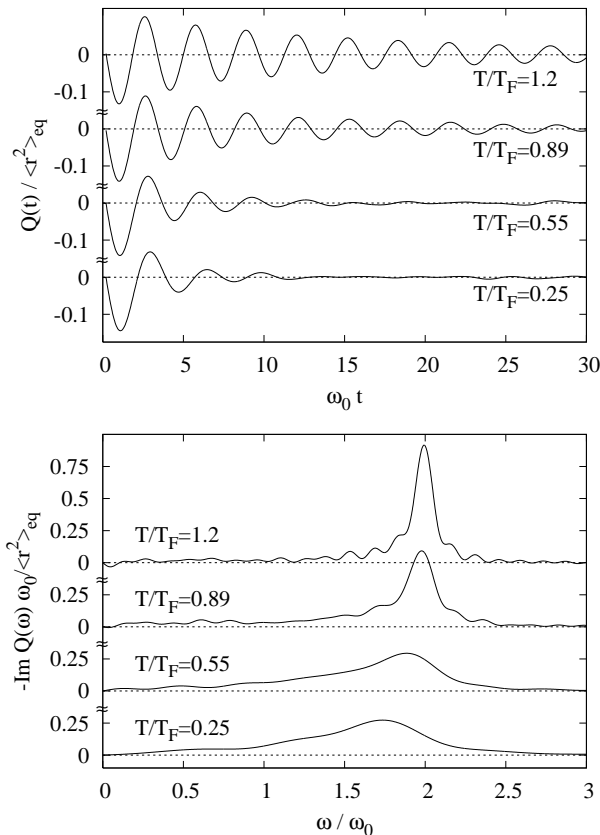


FIG. 4: Upper panel: Quadrupole response to a perturbation of the form (28) with $c = 0.2m\omega_0$ for different temperatures. The system has $N = 10000$ atoms and $1/k_F a = -0.5$. Lower panel: imaginary part of the corresponding Fourier transforms.

We write the perturbation as

$$\hat{V}_1(\mathbf{r}) = \frac{c}{2}(x^2 - y^2), \quad (28)$$

corresponding to a kick at $t = 0$ of $p_x(0^+) = p_x(0^-) - cx(0)$ and $p_y(0^+) = p_y(0^-) + cy(0)$. The parameter c determines the amplitude of the perturbation. If c is chosen too small, it is difficult to separate the oscillation of the mode from fluctuations; if it is chosen too large, one is not in the linear-response regime. All the following results were obtained with $c = 0.2m\omega_0$, corresponding to moderate amplitudes. By varying c within reasonable limits, we checked that the amplitude of the resulting oscillation scales linearly with c .

After the excitation of the radial quadrupole mode, we can look at the time evolution of the quadrupole moment $Q = \langle x^2 \rangle - \langle y^2 \rangle$ as a function of time. Results for different temperatures are displayed in Fig. 4. Contrary to the sloshing and breathing modes, the quadrupole mode is damped and the system approaches equilibrium ($Q \rightarrow 0$) after a certain time. At high temperatures ($T/T_F \gtrsim 1$), the system gets so dilute that it is in the collisionless regime ($\omega_0\tau_{\text{coll}} \gg 1$, τ_{coll} being the mean time between

collisions of one atom). In this case, it takes many oscillations before the system returns to equilibrium. For lower temperatures, the mode is damped because of the high collision rate ($\omega_0\tau_{\text{coll}} \sim 1$), but the system is not yet in the hydrodynamic regime ($\omega_0\tau_{\text{coll}} \ll 1$) where the mode would become undamped again.

For the analysis of the results, it is useful to apply a Fourier transform

$$Q(\omega) = \int_0^\infty dt Q(t) e^{i\omega t}. \quad (29)$$

The so-called response function is the imaginary part of $Q(\omega)$ and can easily be obtained from the numerical results for $Q(t)$ by using a fast Fourier transform (FFT) algorithm [26]. As an example, the Fourier transforms of the results discussed above are shown in the lower panel of Fig. 4. From the Fourier transform one can clearly see that the spectrum of the mode in the collisionless regime, i.e., at high temperature, has a sharp maximum at $\omega = 2\omega_0$, as it should be in an ideal Fermi gas, whereas at lower temperature the spectrum is broadened and the centroid of the spectrum is shifted to lower frequencies. This can be understood since at lower temperature the system is closer to the hydrodynamic regime, where the frequency should be $\omega = \sqrt{2}\omega_0$.

Of course, one would like to give numbers ω_q and Γ_q corresponding to the frequency and damping rate of the quadrupole mode in order to quantify these effects. The simplest way to obtain such numbers would be to fit the response function $Q(t)$ with a damped oscillation of the form $-Ae^{-\Gamma_q t} \sin \omega_q t$. However, in the case of strong damping, this ansatz fits very badly the numerical results for $Q(t)$. This can be understood by looking at the Fourier transforms: The Fourier transform of this ansatz function is a Lorentzian, which has a line shape quite different from that obtained in our numerical simulation for $T/T_F = 0.25$ or 0.55 , cf. lower panel of Fig. 4. Hence, in order to analyze our numerical results, we need some physically motivated ansatz for the fit.

E. Comparison with the method of moments

In most of the theoretical work on collective modes in normal-fluid Fermi gases, the Boltzmann equation was not solved numerically, but approximate analytical solutions were found with the help of the method of moments [6, 17–19]. For a detailed description of the method, see e.g. Ref. [19].

Applying the method of moments to the case of a perturbation of the form (25) with \hat{V}_1 according to Eq. (28), one obtains a theoretical prediction for the response function $\text{Im} Q(\omega)$. A brief description of the derivation is given in Appendix B, the final result reads

$$\text{Im} Q(\omega) = -c \frac{8\langle E \rangle}{3m^2} \frac{\omega\tau}{(\omega^2 - 2\omega_0^2)^2 + \omega^2\tau^2(\omega^2 - 4\omega_0^2)^2}, \quad (30)$$

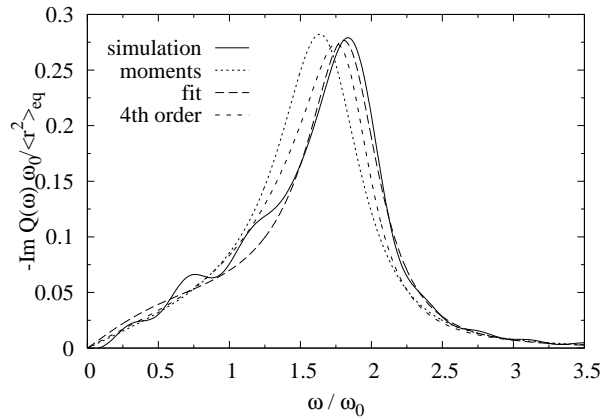


FIG. 5: Fourier transform of the numerical simulation of the quadrupole response (solid line) compared with Eq. (30) where the parameter τ is obtained by the method of moments (dots), or by a fit to the simulation (long dashes). The short dashes represent the response obtained with the extended method of moments including fourth-order moments. The system is a gas of $N = 10000$ particles at $T = 0.4 T_F$ and $1/k_F a = -0.5$.

where $\langle E \rangle = m\omega_0^2 \langle r^2 \rangle$ is the mean energy per atom in equilibrium, and τ is the relaxation time as defined in Refs. [18, 19], and depends on the cross section (i.e., the interaction strength), and the equilibrium distributions, cf. Eq. (B11). One can see from Eq. (30) that in the collisionless and hydrodynamic limits the quadrupole mode has the frequencies $\omega = 2\omega_0$ and $\omega = \sqrt{2}\omega_0$, respectively. The shape of the response function is completely determined by a single parameter, τ .

By looking for the poles of Eq. (30), one can calculate the inverse Fourier transform which gives $Q(t)$. The result has the form

$$Q(t) = -Ae^{-\Gamma_q t} \sin \omega_q t + B(e^{-\Gamma_q t} \cos \omega_q t - e^{-\Gamma_1 t}), \quad (31)$$

i.e., it is a superposition of a damped oscillation with frequency ω_q and damping Γ_q , and a non-oscillating, exponentially decaying term. The explicit expressions for Γ_1 , Γ_q , and ω_q as functions of τ as well as for the amplitudes A and B are given in Appendix C. We will refer to ω_q and Γ_q as the frequency and damping rate of the quadrupole mode. Note that in experiments determining these quantities, the data are usually fitted with a function that is similar to Eq. (31) [4].

In Fig. 5 we compare the response function obtained from the numerical simulation (solid line) with the result obtained from the method of moments, Eq. (30) (dotted line). As one can see, the height of the peak and its general shape are in good agreement, but the position of the maximum is at different frequencies. However, if we try to fit the numerical result with a function of the form of Eq. (30), using τ as fitting parameter, we can very well reproduce the numerical response function (long-dashed line). It is remarkable that by adjusting only one parameter, τ , one can simultaneously reproduce the position,

TABLE I: Relaxation time, frequency, and damping of the quadrupole mode as obtained from the method of moments and fitting the results of the numerical simulation with a function of the form (30), corresponding to the dotted and dashed curves in Fig. 5.

method	$\omega_0 \tau$	ω_q / ω_0	Γ_q / ω_0
moments	0.451	1.676	0.353
simulation	0.587	1.787	0.336

the height and the width of the peak, and also the shape far away from the maximum. However, surprisingly, the fitted value of τ is larger by approximately 30% than the one obtained by the method of moments. As a consequence, the frequency ω_q and damping rate Γ_q obtained from the fit of the response function deviate significantly from those predicted by the method of moments. These results are summarized in Table I.

In the existing literature [6, 17–19], the method of moments was limited to second-order moments, as described in appendix B. However, as we have seen above, this implies that the system is characterized by a single relaxation time τ , whereas in the spirit of a local-density approximation one would expect that in a trapped system the relaxation time should be position-dependent, $\tau = \tau(\mathbf{r})$. For instance, one could imagine that the gas in the center of the trap is more or less hydrodynamic (short relaxation time), whereas far away from the trap center it gets very dilute and hence collisionless (long relaxation time). In the case of the quadrupole mode, this means that the Fermi-surface deformation is stronger at larger radii than in the trap center. It seems therefore natural to include into the ansatz for the perturbed distribution function in addition to the standard term $\propto p_x^2 - p_y^2$ describing the Fermi-surface deformation, a term $\propto r^2(p_x^2 - p_y^2)$. More generally speaking, we should go beyond the standard approximation to include only second-order moments, and include also fourth-order (or perhaps even higher) moments.

The task of extending the method of moments to the next higher order is in principle straight-forward but in practice very tedious: In the case of the quadrupole mode, the number of moments is increased from three to twelve. Some details are given in appendix D. The resulting response function is shown in Fig. 5 as the short-dashed line. Surprisingly, its shape is still similar, but now the position of the maximum agrees rather well with the result of the numerical simulation (solid line). The agreement is even better at higher temperature (see Fig. 6). This nicely confirms the correctness of our numerical simulation and shows explicitly that the method of moments, if truncated at the lowest order, is insufficient.

By doing calculations for various interaction strengths and temperatures, we found that the relaxation time from the simulation is systematically longer than that from the method of moments (without fourth-order moments), Eq. (B11). Results for weaker and stronger in-

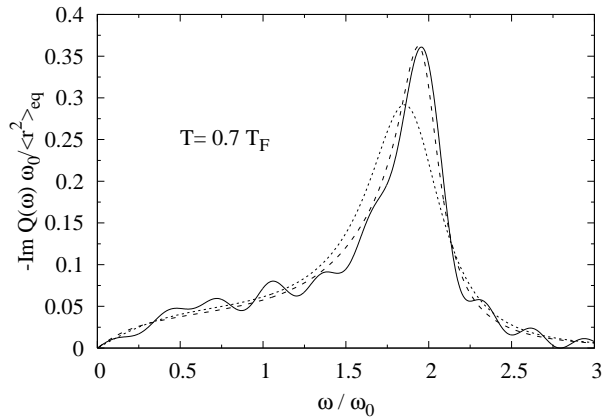


FIG. 6: Same as Fig. 5 for a temperature $T = 0.7 T_F$. For clarity, the fit of the simulation is not shown. The system is a gas of $N = 10000$ particles at $1/k_F a = -0.5$.

interactions ($1/k_F a = -1$ and -0.1) are displayed in Fig. 7. We see that the general behavior of τ as a function of temperature is the same within the simulation and the method of moments, but quantitatively there is a discrepancy of the order of 30% in the whole range of temperatures where our numerical simulation is very accurate ($T > 0.35 T_F$, cf. Fig. 2 showing the temperature dependence of the collision rate). Note that at lower temperatures, the determination of the Pauli-blocking factors in the simulation of the collisions is not completely accurate, as discussed below Fig. 2, such that the collision rate below $0.35 T_F$ is slightly too high. Nevertheless the inverse relaxation time is too small. From this one can conclude that if we could improve the Pauli blocking in the simulation, the discrepancy between the simulation and the method of moments (without fourth-order moments) would be even worse. The fourth order is thus important for the determination of the relaxation of the system and particularly for the frequency and the damping of collective modes.

F. Frequency and damping of the quadrupole mode

As we have just seen, the numerical simulation gives systematically a longer relaxation time τ than the method of moments. As the frequency ω_q and damping rate Γ_q of the quadrupole mode are parametrized in terms of τ (see Appendix Sec. C), one can ask the question how strongly this difference in τ will affect the results for ω_q and Γ_q . Since we are mainly interested in the intermediate regime $\omega\tau \sim 1$ between the hydrodynamic and collisionless limits, a difference of 30% in τ can completely change the temperature dependence of ω_q and Γ_q . This is shown in Fig. 8, where the crosses are the results obtained from the simulation, whereas the solid lines are the results from the method of moments. One can clearly see that the numerical results stay close to

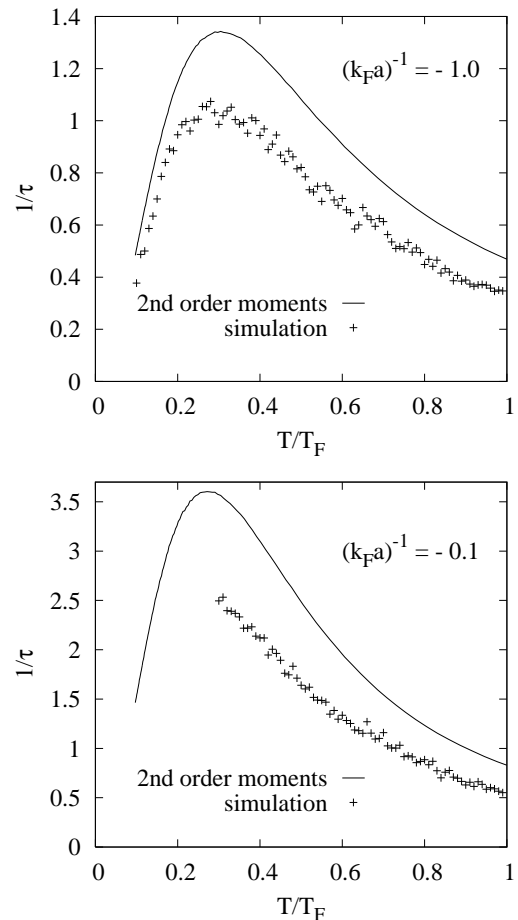


FIG. 7: Comparison of the inverse relaxation time, $1/\tau$, as obtained from the simulation (crosses) and from the method of moments Eq. (B11) (solid lines), as a function of temperature. The system consists of $N = 10000$ atoms with $1/k_F a = -1$ (upper panel) and -0.1 (lower panel).

the collisionless limit to much lower temperatures than the results obtained by the method of moments.

To estimate the resulting precision of our numerical result on ω_q and Γ_q , we show in Fig. 8 the error bands (short-dashed lines) which we obtain if we assume that our simulation may give a τ which is wrong by at most 15%. This error includes numerical uncertainties which can be estimated from the scattering of the points in Fig. 7 and the systematic deviation of the collision rate shown in Fig. 2.

If we include the fourth order moments, a global relaxation time τ does not exist anymore but we could define an effective one by fitting the response function as we did for the simulation. This effective relaxation time agrees very well with the one of the simulation so that both results give very similar frequency and damping. However, from a theoretical point of view, the definition of these quantities should come from the zeroes of the determinant of the matrix A_{ij} defined in Appendix D. Such a discussion is postponed to a forthcoming publication [29].

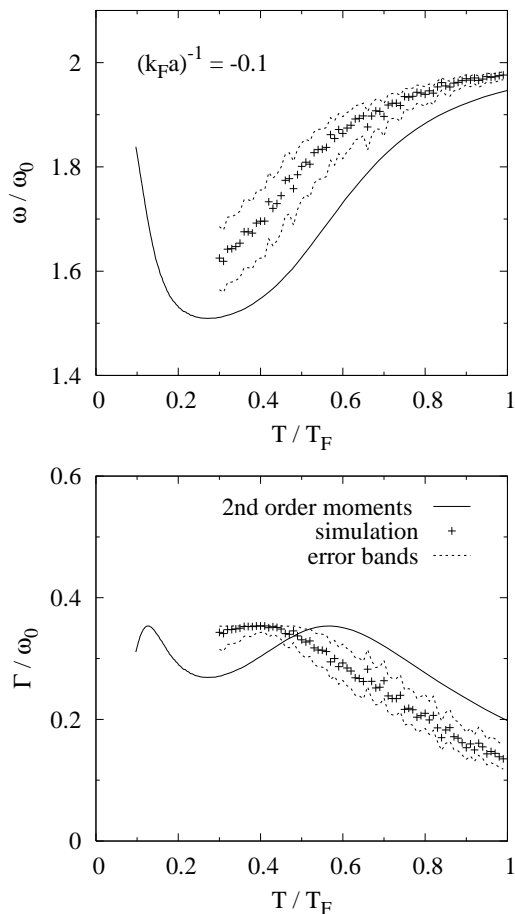


FIG. 8: Frequency (top) and damping rate (bottom) of the quadrupole mode as a function of the temperature as obtained from the numerical simulation (crosses) and from the method of moments (solid line). The short-dashed lines indicate the error band of the results from the simulation if we admit that the relaxation time τ of the simulation may be wrong by 15%. The system consists of $N = 10000$ particles close to unitarity ($1/k_F a = -0.1$).

IV. CONCLUSIONS

In this paper, we presented a test-particle method for solving numerically the Boltzmann equation for trapped Fermi gases. While such methods have been popular in other fields of physics for many years, there have been only a few applications to ultracold atomic gases [14–16, 21]. Our method is similar to that of Refs. [15, 16] with some differences in the treatment of the collision term. In order to compute the occupation numbers in the Pauli-blocking factors in the collision term, we represent each test particle by a Gaussian in \mathbf{r} and \mathbf{p} space. The minimum value of the width of the Gaussian is dictated by the statistical fluctuations due to the finite number of test particles, limiting the applicability of the method to temperatures above $\sim 0.2 T_F$.

As a first application of the method we discussed some

collective modes. For simplicity, we considered only toy systems consisting of $\sim 10^4$ atoms in a spherical harmonic trap and neglected the mean-field potential and medium modifications of the cross section. As expected, the sloshing and monopole modes are undamped and independent of the collisions. In contrast, the quadrupole mode is very sensitive to collisions. In the hydrodynamic limit, its frequency should approach $\sqrt{2}\omega_0$, while it is $2\omega_0$ in the collisionless limit. In our simulations, we never reach the hydrodynamic regime, but the collisionless regime can be realized at high temperature due to the diluteness of the gas.

Surprisingly, the frequency and damping rate of the quadrupole mode obtained within the numerical simulation are quite different from those obtained within the widely used method of moments including moments up to second order in \mathbf{r} and \mathbf{p} . The method of moments predicts a relaxation time τ which is significantly shorter than the one obtained within the simulation. The reason is that the \mathbf{r} dependence of the relaxation time is neglected if only the $p_x^2 - p_y^2$ moment is taken into account for the description of the Fermi-surface deformation. We have shown that if the method of moments is extended to moments up to fourth order in \mathbf{r} and \mathbf{p} , e.g., the $r^2(p_x^2 - p_y^2)$ moment, the agreement with the simulation becomes very good.

The focus of the present paper was mainly to explain the test-particle method and to show its usefulness. For instance, the deficiency of the method of moments up to second order would not have been detected without the comparison with the numerical result. In future studies, we plan to apply the method to more realistic cases. In particular, in order to reach the typical numbers of atoms in the experiments, we will have to increase N by a factor of $\sim 10 - 100$. However, this should not pose a big problem: According to Eq. (10), if we increase N but keep the ratio T/T_F fixed, the widths w_r and w_p may be chosen larger ($\propto N^{1/6}$). This means that Eq. (9) stays satisfied with the same number of test particles, \tilde{N} , i.e., with a reduced ratio \tilde{N}/N . The computation time will only grow because of the increased collision rate (due to the larger test-particle cross section $\tilde{\sigma} = \sigma N/2\tilde{N}$). Another point is the trap geometry. The traps in the experiments are usually not spherical, but elongated. Concerning the propagation of the test particles, this does not cause any difficulty, but in the calculation of the occupation numbers, it will probably be necessary to replace the width w_r of the Gaussian in \mathbf{r} space by different widths w_x , w_y , and w_z in the three space directions. Another important advantage of the numerical method is that an anharmonicity of the trap potential, which is always present in real experiments, can easily be included.

Finally, the mean field [19] and medium modifications of the cross section [6, 19] should be included. The mean field, which originally depends on the chemical potential μ and the temperature T , can be expressed as a function of the local density and energy density, which are both obtainable in the simulation. However,

as shown previously [19], the mean field is not just proportional to the density: this leads to a huge numerical effort which is beyond the scope of this paper. The in-medium cross section is also difficult to be included because it depends on too many variables to be tabulated: $\sigma = \sigma(k = |\mathbf{p} + \mathbf{p}_1|/2, q = |\mathbf{p} - \mathbf{p}_1|; \mu, T)$. One possible solution of this problem is to replace the full k and q dependence of the in-medium cross section by a simple parametrization which results in the same local relaxation time $\tau(\mu, T)$. Work in this direction is already in progress. In Refs. [6, 19], within the method of moments up to second order, the use of the in-medium cross section spoiled the agreement with experimental data because the resulting relaxation times were too short. Since the present work shows that the numerical simulation gives a longer relaxation time than the method of moments, we hope that this problem can be solved.

Further important extensions of the present work are the generalization to polarized Fermi gases and to superfluid systems. These questions, however, require more fundamental theoretical studies before they can be tackled numerically.

Appendix A: Collision rate at equilibrium

Replacing the distribution functions in Eq. (19) by equilibrium distribution functions f_{eq} , one obtains after some algebra the equilibrium collision rate

$$\dot{N}_{coll,eq} = \frac{1}{4\pi^4} \int d^3r \int_0^\infty dk k^2 \int_0^\infty dq q^2 \frac{2q}{m} \sigma(q) \times \left(\frac{\tanh^{-1}(\tanh \frac{X}{2} \tanh \frac{Y}{2})}{Y \sinh X} \right)^2, \quad (\text{A1})$$

where $\mathbf{k} = \mathbf{p} + \mathbf{p}_1$, $\mathbf{q} = (\mathbf{p} - \mathbf{p}_1)/2$, $X = \beta(k^2/8m + q^2/2m + V_T - \mu)$ and $Y = \beta kq/2m$. The total rate of allowed and blocked collisions is, in turn, given by Eq. (19) but without the factor $(1 - f')(1 - f'_1)$ in the integrand, leading to

$$\dot{N}_{coll,eq}^{(+\text{blocked})} = \frac{1}{4\pi^4} \int d^3r \int_0^\infty dk k^2 \int_0^\infty dq q^2 \frac{2q}{m} \sigma(q) \times \frac{\tanh^{-1}(\tanh \frac{X}{2} \tanh \frac{Y}{2})}{Y e^X \sinh X}. \quad (\text{A2})$$

If the trap potential is spherically symmetric or harmonic, the spatial integrals can be reduced to one-dimensional ones. The remaining three-dimensional integrals are evaluated numerically with a Monte-Carlo algorithm.

Appendix B: Quadrupole response within the method of moments

In the case of a weak perturbation, we can write the deviation of the distribution function from the equilibrium

one in the form

$$f - f_{eq} = f_{eq}(1 - f_{eq})\Phi(\mathbf{r}, \mathbf{p}, t). \quad (\text{B1})$$

Inserting this expression into the Boltzmann equation and keeping only terms linear in the perturbation, one obtains (see Eq. (36) of Ref. [19], for the case without mean field but with an external perturbation):

$$f_{eq}(1 - f_{eq}) \left(\dot{\Phi} + \frac{\mathbf{p}}{m} \cdot \nabla_r \Phi - \nabla_r V_T \cdot \nabla_p \Phi + \beta \frac{\mathbf{p}}{m} \cdot \nabla_r V_1 \right) = -I[\Phi]. \quad (\text{B2})$$

Here, $I[\Phi]$ is the linearized collision term as defined in Eq. (37) of Ref. [19] (up to a factor $(2\pi)^3$ since here we are using a different normalization of f):

$$I[\Phi] = \int \frac{d^3p_1}{(2\pi)^3} \int d\Omega \frac{d\sigma}{d\Omega} |\mathbf{v} - \mathbf{v}_1| f_{eq} f_{eq1} \times (1 - f'_{eq})(1 - f'_{eq1})(\Phi + \Phi_1 - \Phi' - \Phi'_1). \quad (\text{B3})$$

The perturbation V_1 is given by Eqs. (25) and (28). The usual approximation consists in making the ansatz

$$\Phi(\mathbf{r}, \mathbf{p}, t) = \sum_{i=1}^3 c_i(t) \phi_i(\mathbf{r}, \mathbf{p}), \quad (\text{B4})$$

with time-dependent coefficients c_i and $\phi_1 = x^2 - y^2$, $\phi_2 = xp_x - yp_y$, and $\phi_3 = p_x^2 - p_y^2$, i.e., only quadratic moments are considered. Evaluating the moments $\int d^3r d^3p \phi_i(\mathbf{r}, \mathbf{p}) \times \text{Eq. (B2)}$, one obtains a system of equations for the Fourier transformed coefficients:

$$\sum_{j=1}^3 A_{ij} c_j(\omega) = a_i \quad (\text{B5})$$

with

$$A_{ij} = \int \frac{d^3r d^3p}{(2\pi)^3} \phi_i \left[f_{eq}(1 - f_{eq}) \times \left(-i\omega \phi_j + \left\{ \phi_j, \frac{p^2}{2m} + \frac{m\omega_0^2 r^2}{2} \right\} \right) + I[\phi_j] \right] \quad (\text{B6})$$

and

$$a_i = -\beta \int \frac{d^3r d^3p}{(2\pi)^3} \phi_i f_{eq}(1 - f_{eq}) \frac{\mathbf{p}}{m} \cdot \nabla \hat{V}_1, \quad (\text{B7})$$

where $\{.,.\}$ are the Poisson brackets. Using the virial theorem, we obtain explicitly:

$$-i\omega c_1 - m\omega_0^2 c_2 = 0 \quad (\text{B8})$$

$$2c_1 - im\omega c_2 - 2m^2\omega_0^2 c_3 = -\beta c, \quad (\text{B9})$$

$$c_2 + \left(\frac{1}{\tau} - i\omega \right) m c_3 = 0, \quad (\text{B10})$$

where the relaxation time τ is defined by [6, 19]

$$\frac{1}{\tau} = \frac{3\beta}{m^2 N \langle E_{kin} \rangle} \int \frac{d^3 r d^3 p}{(2\pi)^3} p_x p_y I[p_x p_y]. \quad (\text{B11})$$

Solving this system of equations, we find

$$c_1(\omega) = \frac{\beta \omega_0^2 c (1 - i\omega\tau)}{\omega^2 - 2\omega_0^2 - i\omega\tau(\omega^2 - 4\omega_0^2)}. \quad (\text{B12})$$

and similar expressions for c_2 and c_3 . However, only the coefficient c_1 contributes to Q : With Eq. (B1), and using again the virial theorem, we obtain $Q(t) = \langle x^2 - y^2 \rangle = 4T \langle r^2 \rangle c_1(t) / 3m\omega_0^2$, or explicitly:

$$Q(\omega) = \frac{4 \langle r^2 \rangle c}{3m} \frac{1 - i\omega\tau}{\omega^2 - 2\omega_0^2 - i\omega\tau(\omega^2 - 4\omega_0^2)}. \quad (\text{B13})$$

Taking the imaginary part, we obtain Eq. (30).

Appendix C: Time dependence of the quadrupole response within the method of moments

In order to compute the Fourier transform of Eq. (B13), let us start by factorizing the denominator:

$$\begin{aligned} \omega^2 - 2\omega_0^2 - i\omega\tau(\omega^2 - 4\omega_0^2) \\ = -i\tau(\omega - \omega_1)(\omega - \omega_2)(\omega - \omega_3). \end{aligned} \quad (\text{C1})$$

The expressions for the roots ω_i can be given in closed form. Defining $\tilde{\tau} = \omega_0\tau$ and

$$\Theta = \left(1 + 9\tilde{\tau}^2 + 3\tilde{\tau}\sqrt{6 - 39\tilde{\tau}^2 + 192\tilde{\tau}^4}\right)^{1/3}, \quad (\text{C2})$$

$$u_{\pm} = \frac{1}{3\tilde{\tau}} \left(\Theta \pm \frac{1 - 12\tilde{\tau}^2}{\Theta} \right), \quad (\text{C3})$$

we can write the roots ω_i as

$$\omega_1 = -i\Gamma_1, \quad \omega_2 = \omega_q - i\Gamma_q, \quad \omega_3 = -\omega_q - i\Gamma_q, \quad (\text{C4})$$

with

$$\Gamma_1 = \frac{1}{3\tilde{\tau}} + u_+, \quad \Gamma_q = \frac{1}{3\tilde{\tau}} - \frac{u_+}{2}, \quad \omega_q = \frac{\sqrt{3}}{2} u_-. \quad (\text{C5})$$

Now it is straight-forward to evaluate the inverse Fourier transform of the response (30) using the residue theorem. The result is given by Eq. (31) with

$$A = \frac{4c \langle r^2 \rangle}{3m\omega_q\tau} \frac{\omega_q^2\tau + (\Gamma_1 - \Gamma_q)(1 - \Gamma_q\tau)}{\omega_q^2 + (\Gamma_q - \Gamma_1)^2}, \quad (\text{C6})$$

$$B = \frac{4c \langle r^2 \rangle}{3m\tau} \frac{1 - \Gamma_1\tau}{\omega_q^2 + (\Gamma_q - \Gamma_1)^2}. \quad (\text{C7})$$

Appendix D: Extension of the method of moments to fourth-order moments

Taking fourth order moments into account, we extend the previous ansatz Eq. (B4) as follows:

$$\begin{aligned} \Phi = & c_1(x^2 - y^2) + c_2(xp_x - yp_y) + c_3(p_x^2 - p_y^2) \\ & + c_4r^2(x^2 - y^2) + c_5p^2(x^2 - y^2) + c_6\mathbf{r} \cdot \mathbf{p}(x^2 - y^2) \\ & + c_7r^2(xp_x - yp_y) + c_8p^2(xp_x - yp_y) \\ & + c_9\mathbf{r} \cdot \mathbf{p}(xp_x - yp_y) + c_{10}r^2(p_x^2 - p_y^2) \\ & + c_{11}p^2(p_x^2 - p_y^2) + c_{12}\mathbf{r} \cdot \mathbf{p}(p_x^2 - p_y^2) \end{aligned} \quad (\text{D1})$$

which can be written as $\Phi = \sum_{i=1}^{12} c_i \phi_i$ with, for example, $\phi_1 = (x^2 - y^2)$. Following the same steps as explained in Appendix B, we obtain now a system of twelve equations. The matrix A_{ij} can be computed explicitly. Contrary to the second order calculations, the virial theorem can no longer be used to reduce the number of unknown quantities so that the system now depends on $\langle r^2 \rangle$, $\langle r^4 \rangle$ and $\langle r^6 \rangle$. In the matrix elements of the collision term, more parameters appear, generalizing the single parameter τ of the second order method.

After solving the system of equations numerically, we can express the quadrupole moment in terms of the coefficients c_i as :

$$Q(\omega) = \frac{4T}{3} \left[\frac{\langle r^2 \rangle}{m\omega_0^2} c_1 + \frac{\langle r^4 \rangle}{5} \left(\frac{7c_4}{m\omega_0^2} + 3mc_5 + mc_9 \right) \right]. \quad (\text{D2})$$

Further details and explicit formula for the matrix can be found in [29].

[1] J. Kinast, S.L. Hemmer, M.E. Gehm, A. Turlapov, and J.E. Thomas, Phys. Rev. Lett. **92**, 150402 (2004).
[2] J. Kinast, A. Turlapov, and J.E. Thomas, Phys. Rev. A **70**, 051401(R) (2004).
[3] M. Bartenstein, A. Altmeyer, S. Riedl, S. Jochim, C. Chin, J.H. Denschlag, and R. Grimm, Phys. Rev. Lett. **92**, 203201 (2004).
[4] A. Altmeyer, S. Riedl, M.J. Wright, C. Kohstall, J.H. Denschlag, and R. Grimm, Phys. Rev. A **76**, 033610 (2007).

[5] A. Altmeyer, S. Riedl, C. Kohstall, M.J. Wright, R. Geursen, M. Bartenstein, C. Chin, J.H. Denschlag, and R. Grimm, Phys. Rev. Lett. **98**, 040401 (2007).
[6] S. Riedl, E.R. Sanchez Guajardo, C. Kohstall, A. Altmeyer, M.J. Wright, J.H. Denschlag, R. Grimm, G.M. Bruun, and H. Smith, Phys. Rev. A **78**, 053609 (2008).
[7] S. Nascimbène, N. Navon, K.J. Jiang, L. Tarruell, M. Teichmann, J. McKeever, F. Chevy, and C. Salomon, Phys. Rev. Lett. **103**, 170402 (2009).
[8] M. Zwierlein, talk given at the conference BEC 2009,

- Sant Feliu de Guixols (Spain), Sept. 5 - 11, 2009.
- [9] C. Menotti, P. Pedri, and S. Stringari, Phys. Rev. Lett. **89**, 250402 (2002).
 - [10] M. Cozzini and S. Stringari, Phys. Rev. Lett. **91**, 070401 (2003).
 - [11] P. Pedri, D. Guéry-Odelin, and S. Stringari, Phys. Rev. A **68** 043608 (2003).
 - [12] E. Taylor and A. Griffin, Phys. Rev. A **72**, 053630 (2005).
 - [13] M. Urban and P. Schuck, Phys. Rev. A **73**, 013621 (2006).
 - [14] M. Urban, Phys. Rev. A **75**, 053607 (2007), Phys. Rev. A **78**, 053619 (2008).
 - [15] F. Toschi, P. Vignolo, S. Succi, and M.P. Tosi, Phys. Rev. A **67**, 041605(R) (2003).
 - [16] F. Toschi, P. Capuzzi, S. Succi, P. Vignolo, and M.P. Tosi, J. Phys. B **37**, S91 (2004).
 - [17] P. Massignan, G.M. Bruun, and H. Smith, Phys. Rev. A **71**, 033607 (2005).
 - [18] G.M. Bruun and H. Smith, Phys. Rev. A **76**, 045602 (2007)
 - [19] S. Chiacchiera, T. Lepers, D. Davesne and M. Urban, Phys. Rev. A **79**, 033613 (2009).
 - [20] G.F. Bertsch and S. Das Gupta, Phys. Rep. **160**, 189 (1988).
 - [21] B. Jackson and E. Zaremba, Phys. Rev. A **66**, 033606 (2002).
 - [22] E.M. Lifshitz and L.P. Pitaevskii, *Physical Kinetics*, L.D. Landau and E.M. Lifshitz Course of Theoretical Physics Vol. 10 (Pergamon, Oxford, 1980).
 - [23] L.D. Landau and E.M. Lifshitz, *Quantum Mechanics*, Course of Theoretical Physics Vol. 3 (Pergamon, London, 1958).
 - [24] W.C. Swope, H.C. Andersen, P.H. Berens, and K.R. Wilson, J. Chem. Phys. **76**, 637 (1982).
 - [25] L. Verlet, Phys. Rev. **159**, 98 (1967).
 - [26] W.H. Press, S.A. Teukolsky, W.T. Vetterling, and B.P. Flannery, *Numerical Recipes in FORTRAN: The Art of Scientific Computing*, 2nd edition (Cambridge University Press, 1992).
 - [27] W. Kohn, Phys. Rev. **123**, 1242 (1961).
 - [28] L. Brey, N.F. Johnson, and B.I. Halperin, Phys. Rev. B **40**, 10647 (1989).
 - [29] Thomas Lepers, Institut de Physique Nucléaire, Université de Lyon, PhD Thesis, to be published. T. Lepers, S. Chiacchiera, M. Urban, and D. Davesne in preparation.